Send Orders for Reprints to reprints@benthamscience.net

Protein & Peptide Letters, 2013, *20*, 1009-1017

Biophysical Characterization of the Membrane-proximal Ectodomain of the Receptor-type Protein-tyrosine Phosphatase Phogrin

Martín E. Noguera[a,b], María E. Primo[c], Laura N. F. Sosa[c], Valeria A. Risso[a,b], Edgardo Poskus[c], and Mario R. Ermácora[a,b]*

[a]*Departamento de Ciencia y Tecnología, Universidad Nacional de Quilmes, Roque Sáenz Peña 352, B1876BXD Bernal, Buenos Aires, Argentina;* [b]*Imbice-Conicet, Calle 576 y Camino General Belgrano, B1906APO La Plata, Buenos Aires, Argentina;* [c]*Cátedra de Inmunología de la Facultad de Farmacia y Bioquímica, División Endocrinología del Hospital de Clínicas J. de San Martín, Universidad de Buenos Aires (UBA), and IDEHU, Conicet-UBA, Junín 954 C1113AAD, Ciudad Autónoma de Buenos Aires, Argentina*

Abstract: The receptor-type protein-tyrosine phosphatase (RPTP) phogrin is localized at the membrane of secretory granules of pancreatic islet β-cells and, similarly to the closely related ICA512, plays a role in the regulation of insulin secretion, in ensuring proper granulogenesis and stability, and in the regulation of β-cell growth. The mature membrane-proximal ectodomain of phogrin (MPE phogrin) was produced as a recombinant protein and characterized. CD, fluorescence, controlled proteolysis, size-exclusion chromatography, and multi-angle light scattering showed that it is a properly-folded monomeric domain. Equilibrium experiments, in the presence of guanidinium chloride and thermal unfolding, suggest a two-state mechanism with a ΔG of 2.3-3.3 kcal/mol, respectively. The study establishes common features and differences of MPE phogrin and the homologous ectodomain of ICA512. A homology model of phogrin was built based in the x-ray structure of MPE ICA512. The model is a starting point for modeling the entire receptor and for testing the quaternary structure and interactions of this protein *in vivo*. A description of the membrane insertion mode and putative interacting surfaces of this large protein is fundamental for the understanding of its biological function.

Keywords: Diabetes, equilibrium unfolding, homology modeling, phogrin, receptor-type protein-tyrosine phosphatase, secretory granule.

1. INTRODUCTION

Protein hormones and neuropeptides secreted through the regulated pathway are stored in granules and liberated in response to specific stimuli. The cellular machinery and control mechanisms that make possible regulated secretion are of extraordinary complexity and scientific interest.

Among the granule-specific proteins with an important role in the biogenesis, cargo storage, exocytosis and recycling of secretory granules there are two receptor-like protein-tyrosine phosphatases: phogrin (also known as IA-2β, IAR, ICAAR, or RPTPN2) and ICA512 (also known as IA-2, PTP35, or RPTPN). They are related type I transmembrane glycoproteins located in dense core vesicles and mainly expressed in brain, pituitary, pancreatic islet, and adrenal endocrine cells. Both lack tyrosine phosphatase activity as a consequence of mutations at the active site. Recently, however, it was reported that phogrin possesses the ability to dephosphorylate phosphatidylinositol [1].

ICA512 and phogrin were first known as major autoantigens in type-1 diabetes mellitus, and have been widely used for early detection of individual at risk [2-4]. Later, it was learned that they have a role in the regulation of insulin secretion, in ensuring proper granulogenesis and stability, and in the regulation of β-cell growth [5-8]. However, the biological functions of these receptors are still poorly characterized.

In mice, the targeted deletion of ICA512, phogrin, or both, results in mild impairment of glucose-stimulated insulin secretion and abnormal secretion of pituitary hormones and female infertility [9-12]. Although phogrin and ICA512 are closely related, their expression profile is dissimilar: ICA512 expression increases during development [13-15] and is influenced by glucose, insulin, cAMP-generating agents, and proinflammatory cytokines; in contrast, phogrin expression is constant and not significantly affected by glucose levels [15-17].

The precursors of ICA512 and phogrin are polypeptides of about 1000 residues that undergo proteolytic processing by furin like convertases to the ~60-kDa transmembrane mature proteins through the secretory pathway [5, 18]. The mature receptor comprises an extracellular region (oriented toward the lumen of the granule), a transmembrane domain, and a cytoplasmic tail of about 45 kDa. The cytoplasmic tail includes the phosphatase domain that identifies these proteins as members of the RPTP family.

*Address correspondence to this author at the Departamento de Ciencia y Tecnología, Universidad Nacional de Quilmes, Roque Sáenz Peña 352, B1876XD Bernal, Buenos Aires, Argentina. Tel: +54 11 43657100; Fax: +54 11 43657132; E-mail: ermacora@unq.edu.ar

1875-5305/13 $58.00+.00

The extracellular region is exposed to the extracellular milieu during insulin secretion and therefore it is an obvious candidate for the interaction with other membrane proteins and external ligands. At least three proteolytic variants of the mature phogrin extracellular region, with distinct N-termini, were identified in brain cells, but only the shorter form (114 residues) was found in pancreatic β-cells [18]. This form is the closest match to the 127-residue mature extracellular region generated during the proteolytic processing of ICA512.

Recently, we determined the x-ray structure of a structural domain comprising most of the extracellular region of mature ICA512. This 89-residue domain, which we named membrane proximal ectodomain ICA512 (MPE ICA512), is related to the SEA (Sea-urchin sperm protein, Enterokinase, Agrin) family of domains [19-21], which are specialized modules for oligomerization and interaction with the extracellular matrix. This finding simplified the classification of the RPTP family because, with the single exception of the subtype R7 (PCPTP1), all RPTP are now recognized by having extracellular modules for the interaction with the extracellular matrix and cell-to-cell contact [22,23].

The quaternary structure of ICA512 and phogrin has also received considerable attention. There is evidence that the intracellular and transmembrane domains of the receptors have oligomerization potential *per se*, and it has been proposed that association processes mediate several of their functions [24,25]. Homo- and hetero-dimerization are considered important for type I membrane receptors, and particularly for the RPTP family of proteins. The x-ray structure of MPE ICA512 provided a catalog of association modes that may be of functional importance [20]. In addition, previous work provided the basic biophysical information for analyzing the behavior of the MPE ICA512 [26].

Although the structure of MPE phogrin (the phogrin extracellular region equivalent to MPE ICA512) remains to be solved, their sequence similarity is 63%, high enough as to safely assume a common overall fold. Nevertheless, some of the differences in expression, regulation, and function between ICA512 and phogrin might be related to specific sequence changes or subtle structural details and warrant further investigation. To unify and systematize the structural and biophysical information regarding the receptor-like protein-tyrosine phosphatases, we present here hydrodynamic, stability, and molecular modeling studies of MPE phogrin.

2. MATERIALS AND METHODS

2.1. Miscellanea

All chemicals were of the purest analytical grade available. Sodium dodecyl sulphate polyacrylamide gel electrophoresis (SDS-PAGE) was performed according to the method of Schägger and von Jagow [27]. MALDI-TOF mass analysis was performed with a 4800 Plus MALDI-TOF/TOF Analyzer instrument (AB Sciex, Framingham, MA, USA). Phogrin concentration was measured by UV absorbance at 280 nm, the extinction coefficient in the unfolded state was calculated from the amino acid composition [28], and the corresponding value for the native state (ε_{280} = 1300 M^{-1} cm^{-1}) was determined as described [29]. Analytical size-exclusion chromatography (SEC) was carried out on a Jasco HPLC system equipped with a HR 10/30 Superose 12 column (GE Healthcare). Elution buffer was 25 mM sodium phosphate, 150 mM NaCl, pH 7.0, and the absorbance detector was set at 280 nm. Stokes' radii (R_S) were calculated from a calibration curve with standard proteins [30]. Nonlinear least-squares fitting of equations to data was carried out with the Solver add-in of Microsoft Excel 2010®, and errors were calculated by Monte Carlo simulation as described [31].

2.2. Molecular Biology

The phogrin domain studied herein (MPE phogrin) comprises residues 502 to 599 of the precursor protein (UniProt ID: Q92932), and it corresponds by homology to the previously characterized ICA512 domain comprising residues 470 to 558 (UniProt ID: Q16849). DNA encoding MPE phogrin isoform 1 [32] was prepared by PCR using as a template DNA encoding the isoform 2 of the same protein kindly provided by Dr. John C. Hutton from the Barbara Davis Center for Childhood Diabetes, University of Colorado; appropriate primers were used to introduce the 29-residue fragment that is missing in the latter. The prepared DNA was ligated into pET-9b (Novagen, Madison, USA), and the identity of the resulting expression construct, named pIA2BS, was verified by sequencing.

2.3. Protein Expression and Purification

E. coli BL21 (RIL) cells transformed with pIA2BS were cultured in 1 liter of TB medium with 50 μg/ml kanamycin and 34 μg/ml chloramphenicol, and phogrin expression was induced at 20 °C and $OD_{600\ nm}$ = 1 with 1% (w/v) lactose for 20 h. After expression, the cells were harvested by centrifugation (7500 × g; 10 min; 4 °C), washed twice with buffer A (25 mM TrisHCl, pH 7.2), and stored at –20°C. Immediately before protein purification, the cells were thawed, resuspended in 20 ml of buffer A containing 1 mM PMSF, and broken by high pressure (1000 psi) with a French Press (Thermo Electron Corporation, Waltham, MA, USA). Cell debris was removed by centrifugation (20,000 × g, 20 min, 4 °C, twice) and the supernatant was subjected to ammonium sulphate precipitation by adding solid ammonium sulphate to 60 % saturation and stirring 30 min on ice. The soluble fraction was separated by centrifugation (10,000 × g, 15 min, 0 °C) and further fractionated by adding solid ammonium sulphate up to 80 % saturation with stirring for 60 min on ice. The final supernatant was separated by centrifugation as above, desalted in a PD10 column (GE Healthcare) and subjected to ionic exchange chromatography on a HR 5/5 Mono Q column (GE Healthcare) equilibrated with buffer A. Fractions containing nearly pure phogrin were isolated using a NaCl gradient in equilibration buffer. Further purification was achieved by size-exclusion chromatography on a HR 10/30 Superose12 column (GE Healthcare) equilibrated in 25 mM sodium phosphate pH 7.0. The product identity was verified by mass analysis.

2.4. Optical Studies

CD spectra were collected on a Jasco 810 spectropolarimeter (Jasco Corporation, Tokyo, Japan) using a 0.1- and

1-cm path-length cell for far-UV and near-UV, respectively. Measurements were carried out at 20 °C, and the sample concentration was 12 and 93 μM for far- and near-UV, respectively. Scan speed was set at 20 and 50 nm/min (near–UV and far–UV, respectively) with 1-s response time, 0.2-nm data pitch and 1-nm bandwidth. Eight to ten scans were averaged for each sample, blank-subtracted, and smoothed using a fourth-degree Savitzky–Golay polynomial filter with a 10-point sliding window [33]. The content of secondary structure was calculated from the far-UV CD spectrum using a suite of programs [34].

Fluorescence emission spectra were collected on an ISS K2 multifrequency phase fluorometer (ISS, Champaign, Illinois, USA) equipped with a cell holder connected to a circulating water bath set at 20 °C. For intrinsic fluorescence, protein concentration was 34 μM, the excitation wavelength was 276 nm, and the intensity of fluorescence emission was measured between 250 and 450 nm. For 1-anilino naphtalene-8-sulfonic acid (ANS, Molecular Probes) binding experiments, aliquots from a 530 μM stock of ANS were added incrementally to the protein solution and the spectrum from 400 to 600 nm was recorded after excitation at 350 nm.

Mass determination by multi-angle light scattering (MALS) was achieved using a miniDawn instrument (Wyatt Technology) coupled to a size-exclusion chromatography system based on a Superdex 200 10/300 GL column (GE Healthcare). The elution buffer was 25 mM sodium phosphate, pH 7.0, 150 mM NaCl. The analysis was performed at 20 °C and with a flow rate of 0.3 ml/min. Data analysis was performed using Astra 6.0 (Wyatt Technology).

2.5. Controlled Proteolysis

MPE phogrin (33 μM) was incubated with trypsin (75:1 mass ratio) in 25 mM sodium phosphate, pH 7.0 at 27 °C. Samples were withdrawn at different times, and digestion was stopped by the addition of SDS-PAGE loading buffer followed by boiling for 5 min and freezing at -20 °C until analysis.

2.6. Thermal Unfolding

Thermal scans at different pH values were collected in the far-UV with a Jasco 810 spectropolarimeter. Ellipticity was measured at 222 nm between 4 and 90 °C with a constant heating rate of 2 °C/min and a 1-cm path-length cell. Protein concentration was 6 μM, in 25 mM sodium phosphate pH 7.0 or 7.5, or 20 mM sodium acetate pH 4.8. To assess the protein concentration dependence of the melting curves the measurement was as above but in 25 mM sodium phosphate pH 7.0 and protein concentration range from 1 to 12 μM.

2.7. Chemical Unfolding

Isothermal unfolding experiments were carried out using the above-described spectropolarimeter, with a 0.1-cm path-length cell, and the scan speed was set at 100 nm/min. Experiments were performed at 20 °C in 25 mM sodium phosphate pH 7.0 and different concentrations of guanidinium chloride (GdmCl). A fresh stock solution of GdmCl approximately 8 M in buffer was prepared for each experiment and the exact denaturant concentration was determined by refractive index measurement, using a Palm Abbe digital refractometer (Misco, Cleveland, OH, USA). Samples were prepared diluting the GdmCl stock solution with buffer, followed by the addition of MPE phogrin, to give final GdmCl concentration from 0 M to 5 M, and final 13 μM protein concentration. Scans were acquired between 210 and 320 nm and smoothed with a non-parametric digital filter implemented in PeakFit, version 4 (SeaSolve Software Inc). Ellipticity at 222 nm was used for monitoring the unfolding transitions.

2.8. Equilibrium Unfolding Data Analysis

For denaturant induced transitions, it was assumed a linear dependence of ΔG with the denaturant concentration [35],

$$\Delta G = \Delta G_0 - mD \tag{1}$$

where ΔG_0 is the Gibbs free energy of unfolding in absence of denaturant, m is the rate of energy change per molar unit of denaturant, and D is the denaturant molar concentration. C_m is the denaturant concentration at which $\Delta G = 0$, and therefore

$$\Delta G = m(C_m - D) \tag{2}$$

A two-state unimolecular unfolding model was assumed, N↔U, where the observed instrument signal (S) was modeled as a sum of intrinsic signals from each of the states in the equilibrium:

$$S = (S_{0,N} + l_N D)(1 - f_U) + (S_{0,U} + l_U D) f_U \tag{3}$$

where S is the sum of the molar fraction of the unfolded (f_U) and native state ($1\text{-}f_U$), multiplied by the native and unfolded signals, which vary linearly with the denaturant concentration to account for the pre- and post-transitions baselines, S_0 is the intrinsic signal for each state in absence of denaturant, and l is the denaturant dependence of the signal for each state with denaturant concentration.

The final fitting equation can be obtained combining the above equations:

$$S = \frac{(S_{0,N} + l_N D) + (S_{0,U} + l_U D)\exp\{mD - C_m)/RT\}}{1 + \exp\{mD - C_m)/RT\}} \tag{4}$$

The following equations were used for thermal transitions:

$$\Delta G_T = -RT \ln\left(\frac{f_U}{f_N}\right) = \Delta H_{T_m} + \Delta C_p (T - T_m) - T\left[\frac{\Delta H_{T_m}}{T_m} + \Delta C_p \ln\left(\frac{T}{T_m}\right)\right] \tag{5}$$

where T_m is the temperature at which $\Delta G = 0$. Native and unfolded fractions were obtained from the spectroscopic signal using an expression similar to Eq. 3, where native and unfolded signals were assumed to vary linearly with temperature.

Data sets for unfolding at different pH were modeled with a global ΔC_P and pH-specific T_m. ΔH at each pH was not an independent parameter but was calculated as

$$\Delta H_{pH=j} = \Delta H_{pH=7.0} + \Delta C_p (T_{m,pH=j} - T_{m,pH=7.0}) \quad (6)$$

This ensures that ΔH varies linearly and identically with temperature [36] for all the tested pH and reduces the number of adjustable parameters.

2.9. Homology Modeling

The model of monomeric MPE phogrin was based on the crystal structure of the homologous mature ectodomain of ICA512 (PDB ID: 2qt7 and 3np5) [19-20] and built with Coot [37]. Rotamers were optimized using the library provided in Coot and energy minimization. The final quality of the model was evaluated with Procheck [38] and MolProbity [39].

3. RESULTS AND DISCUSSION

3.1. Expression properties and covalent structure

MPE phogrin was expressed efficiently as a soluble protein in *E. coli*, and judging from SDS-PAGE analysis, the purification procedure yielded large amounts of 99 % pure protein. The experimental mass of the product was 10811.4 Da within 2.0 Da of the theoretical mass calculated from the sequence. However, the SDS-PAGE mobility of the protein is somewhat slower than expected (not shown), corresponding to a 12.5-M_r protein. The causes for this behavior were not investigated, but it might be related to sequence peculiarities.

3.2. Hydrodynamic Behavior and Optical Properties

The apparent R_S and molecular mass calculated for MPE phogrin from the chromatographic elution times in SEC are 22.5 ± 0.3 Å and 22.5 ± 0.9 kDa, respectively (Fig. **1**, Panel **A**). The elution time does not change with sample concentration in the 2-250 μM range (not shown), and judging from the chromatograms, the amount of higher order aggregates is negligible. The SEC results suggest a dimeric structure with a very small dissociation constant. However, the hydrodynamic parameters of a protein derived from elution times in SEC experiments depend on molecular shape and are susceptible to artifacts from protein-matrix interactions. To assess the mass of the particle in solution by a direct method, a SEC run using a column packed with a different matrix was analyzed by multi-angle light scattering (Fig **1**, Panel **B**). The mass of MPE phogrin deduced by this procedure is 10.8 kDa, which is consistent with a monomeric state. Moreover, the elution time of MPE phogrin in the SEC monitored by MALS is consistent with a monomer (not shown). From the two analyses, we conclude that MPE phogrin is a monomer in solution and that the anomalous behavior of MPE phogrin in the SEC experiment shown in (Fig. **1**, Panel **A**) is due to a specific interaction of the protein with the Superose 12 matrix.

CD spectra of MPE phogrin are shown in (Fig. **2**), panel A. In the far-UV, two strong minima at 208 and 219 nm and a maximum at 192 nm suggest a significant content of α-helix. Numerical analysis using a variety of methods yields an average content of 32 % of α-helix and 17 % β-strand structure [34]. In the near-UV region (Fig. **2**, panel **B**), the

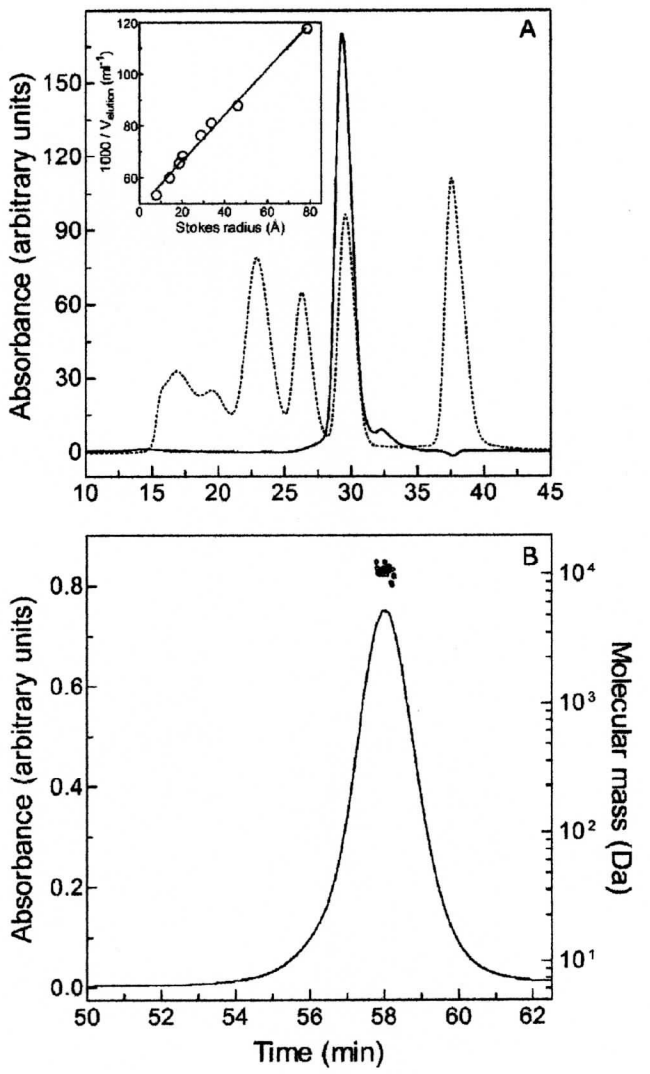

Figure 1. Aggregation state. In Panel **A**, the elution profile of MPE phogrin in a calibrated HR 10/30 Superose 12 column is shown as a solid line. In dotted line, from left to right, the peaks correspond to thyroglobulin (670 kDa, a central peak with two shoulders), bovine IgG (158 kDa), ovalbumin (43 kDa), myoglobin (17 kDa) and vitamin B12 (1.3 kDa), respectively. Elution buffer was 25 mM sodium phosphate, 150 mM NaCl, pH 7.0. The inset shows the calibration curve of the column using the above markers and in addition bovine serum albumin (67 kDa), RNAse A (13.7 kDa), and aprotinin from bovine lung (6.5 KDa). In Panel **B**, the elution profile and mass determination by light scattering (MALS, circles) are shown (see the Material and methods section for the details). In this case a Superdex 200 10/300 GL column was used for SEC.

sharp vibrational structure of the two phenylalanine residues (250-270 nm) indicates a tight tertiary packing of the hydrophobic core. Less pronounced spectral structure is observed in the 275-285 nm region, suggesting a less asymmetric environment for the single tyrosine residue present in the protein. The absence of tryptophan residues is evidenced by the lack of rotatory power above 285 nm.

Fluorescence emission spectra of MPE phogrin are shown in (Fig. **3**). As expected, only tyrosine emission fluo-

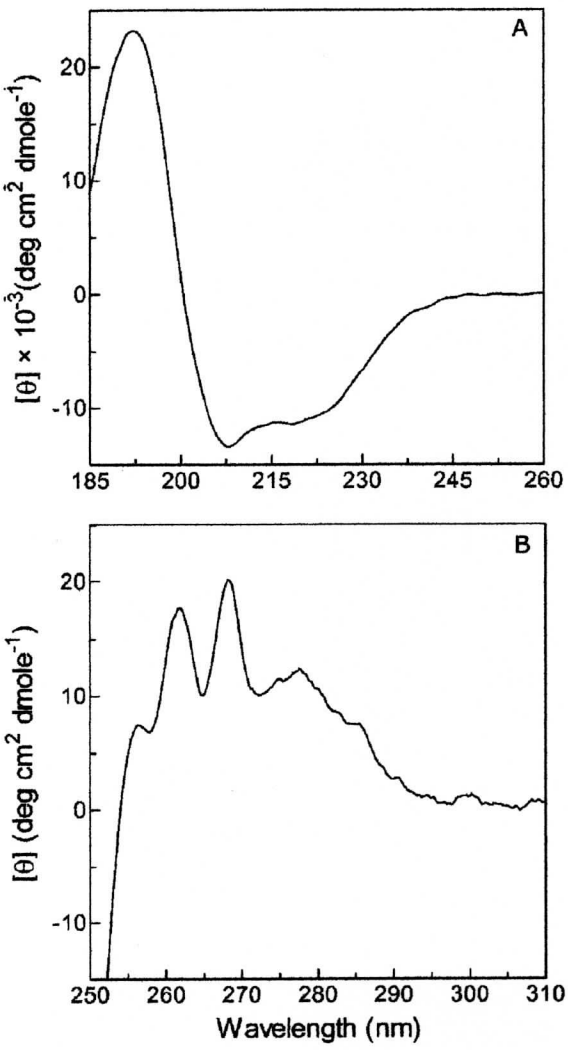

Figure 2. CD spectra of MPE phogrin. Panel **A**, far-UV. Panel **B**, near-UV. Measurements were performed at 20°C in 25 mM sodium phosphate, pH 7.0.

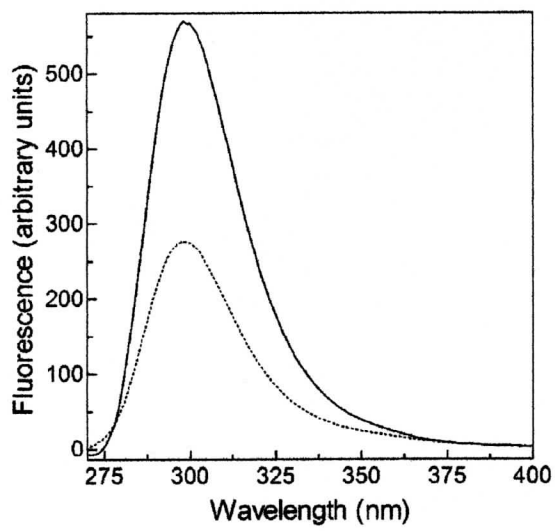

Figure 3. Fluorescence emission spectra of native and unfolded MPE phogrin. Excitation was at 276 nm. Measurements were performed at 20 °C in 25 mM sodium phosphate, pH 7.0 without (solid line) or with (dashed line) 5 M GdmCl.

rescence is observed, and the quantum yield of this fluorescence is strongly decreased by 5 M GdmCl. This behavior can be ascribed to the unfolding of the protein and exposure of the fluorophore to the solvent.

ANS is a fluorescent hydrophobic probe known to bind to partially folded states and to solvent-accessible hydrophobic pockets. In the presence of ANS, the spectra of folded and unfolded protein are similar (not shown), with a maximum at 524 nm, and these spectra are in turn similar to the spectrum in absence of protein. Likewise, no spectral change was detected at intermediate denaturant concentrations. Thus, neither folded nor unfolded MPE phogrin bind ANS, demonstrating the absence of large exposed and hydrophobic cavities or surfaces in the native state. Similarly, the absence of binding in the presence of 5 M GdmCl is an indication of full unfolding of the protein in that condition. At intermediate denaturant concentrations, the absence of ANS binding is congruent with a two state unfolding mechanism with no partially folded states.

The conformational flexibility of MPE phogrin was assessed by controlled proteolysis. As shown in (Fig. **4**), the protein is remarkably resistant to the action of trypsin, despite the fact that it contains 13% of lysine and arginine residues. The resistance to proteolysis is consistent with a well-packed and folded native state.

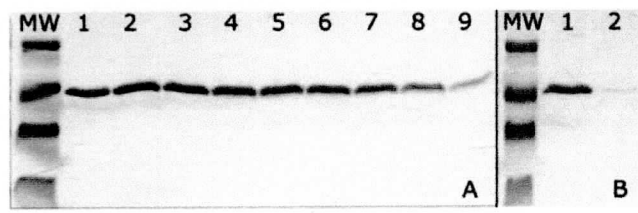

Figure 4. Limited proteolysis of MPE phogrin followed by SDS-PAGE and Coomassie blue staining. Panel **A**, lanes 1-9, MPE phogrin was incubated with trypsin (1:75 w:w) at 27 °C, and aliquots were withdrawn at 1, 2, 5, 10, 15, 20, 30, 40, and 60 min, respectively. Panel **B**, lane 1-2, aliquots withdrawn at 120 min, after incubation without and with protease, respectively. MW, mass markers (20.1, 14.2, 6.5 and 3.5 kDa).

3.3. Thermal Unfolding

To assess the thermodynamic stability of MPE phogrin, equilibrium unfolding experiments were carried out monitoring CD ellipticity while increasing linearly the temperature from 4 to 90 °C (Fig. **5**). The monitored signal reports mostly on the secondary structure content, and the rate of temperature change and the tested protein concentration ranges were chosen as to ensure full recovery of the native signal after cooling from 90 °C to room temperature (not shown). The unfolding model and corresponding equations described in Material and Methods were used for fitting. The thermodynamic parameters derived are shown in Table **1**.

The ΔG associated with the unfolding of MPE phogrin at the temperature of maximum stability is pH-dependent. At pH 4.8, close to the pH of the lumenal compartment in the mature secretion granule, ΔG is 3.3 kcal mol^{-1}. At pH 7.5, close to the pH of the extracellular milieu, ΔG drops to 2.3

Table 1. Thermodynamic parameters for the thermal unfolding of MPE phogrin[a]

pH	T_m[b]	ΔH_{Tm}[c]	ΔC_P	T_x[d]	ΔG_{Tx}[e]
	°C	kcal mol^{-1}	kcal mol^{-1} K^{-1}	°C	kcal mol^{-1}
4.8	66.6 ± 0.1	50.9 ± 0.6	1.10 ± 0.03[f]	23.4 ± 1.3	3.3 ± 1.5
7.0	59.1 ± 0.1	42.6 ± 0.4	1.10 ± 0.03	22.6 ± 1.1	2.4 ± 1.3
7.5	57.9 ± 0.1	41.3 ± 0.4	1.10 ± 0.03	22.5 ± 1.1	2.3 ± 1.2

[a]The parameters were obtained by least-square fitting the equations described in Materials and Methods to the data shown in Figure 5. [b]Temperature at which $\Delta G = 0$ for the unfolding transition. [c]ΔH at T_m. [d]T_x is the temperature at which ΔG is maximum, $\Delta G = \Delta H$, and $\Delta S = 0$. [e]ΔG at T_x. [f]ΔC_P was adjusted globally to the enthalpy at different pH.

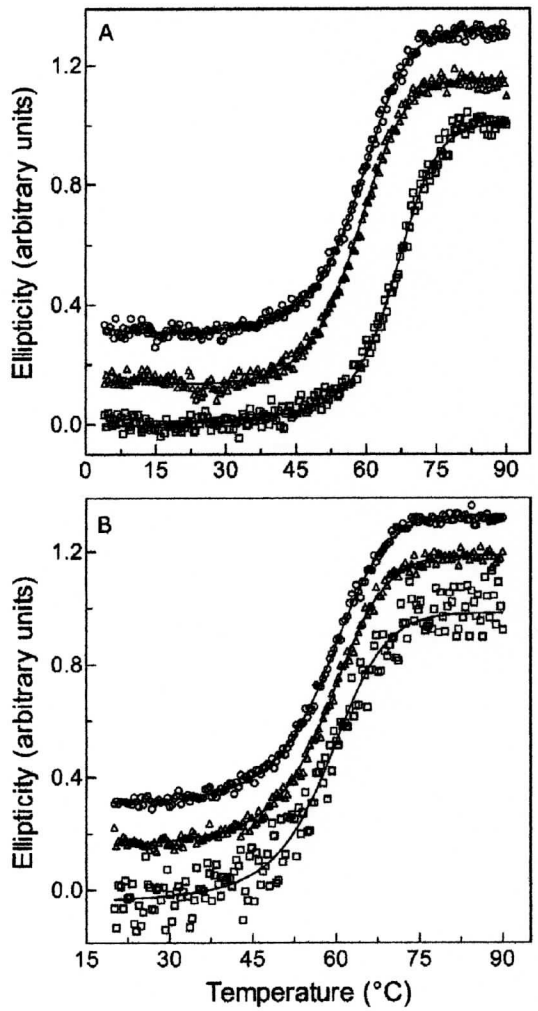

Figure 5. Thermal unfolding of MPE phogrin. For clarity, the data and curves were arbitrarily displaced on the ordinate axis. Transitions were monitored by CD at 220 nm and the signal represents mostly changes in the α-helical content. Panel **A**, transitions at different pH: pH 7.0 (circles), 7.5 (triangles), and 4.8 (squares). Panel **B**, transitions as a function of protein concentration: 12, 5, and 1 μM were represented with circles, triangles, and squares, respectively. Lines represent the global fit of the two-state unimolecular unfolding model (Eq. 5 and 6) to all the experiments (see Table **1**).

kcal mol^{-1}, which is a low stability for native proteins. On the other hand, the ΔC_P value from the fit (1.10 kcal mol^{-1} K^{-1}) is in excellent agreement with the value calculated for a protein of the size of MPE phogrin (1.15 kcal mol^{-1} K^{-1}) [40], which suggests that the melting curves represent full unfolding transitions.

3.4. Isothermal Unfolding

GdmCl is a chemical denaturant that promotes protein unfolding by stabilizing the unfolded state. The GdmCl-induced unfolding of MPE phogrin at 20 °C and pH 7.0 was monitored by CD ellipticity at 220 nm, and the transition curve is shown in (Fig. **6**). Additionally, the hydrodynamic behavior of the protein at different GdmCl concentrations was assessed by SEC. The reversibility of the unfolding was nearly complete judging from the recovery of the signals after refolding (not shown). Based on the results of the thermal unfolding, only a single protein concentration was tested, and data fitting was carried out using two-state unimolecular unfolding model (Eq. 4). The values of the adjusted parameters were m = 3.57 ± 0.22 kcal mol^{-1} M^{-1} and ΔG = 2.29 ± 0.15 kcal mol^{-1}, in excellent agreement with the expected change in solvent accessible surface area and the above thermal unfolding results. The unfolding monitored by SEC followed closely the fit line of the CD data, except for the GdmCl concentrations below 0.5 M GdmCl. As shown

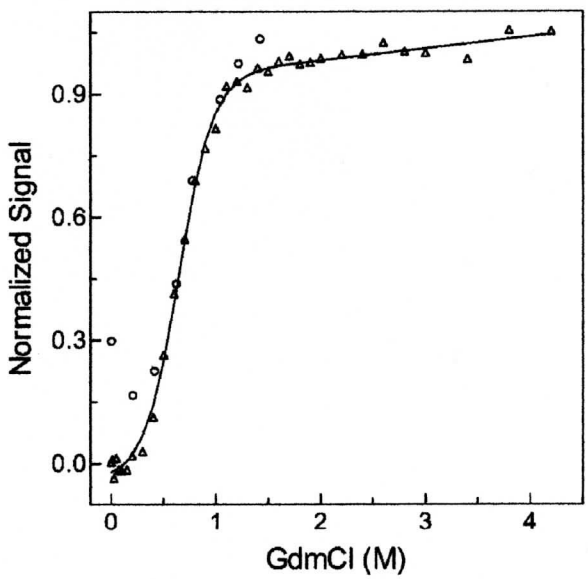

Figure 6. GdmCl-induced unfolding of MPE phogrin. The isothermal transition was monitored by CD at 222 nm (triangles) and SEC (circles). The line is the result of fitting the two-state unimolecular unfolding model (Eq. 4) to the CD data. The derived thermodynamics parameters are given in the text.

above, in absence of denaturant, MPE phogrin behaves anomalously in the Superose column. In the presence of 0.5 M GdmCl, the protein behaves as expected for a monomer and at higher denaturant concentrations expands as expected in a two-state mechanism.

3.5. 3D structure Model

Sequence identity and similarity between MPE ICA512 and phogrin are 40 and 63%, respectively (see (Fig. **S1**) in Supplementary Data). This high degree of similarity allowed a straightforward modeling by threading of the phogrin sequence into the known x-ray structure of MPE ICA512. After local energy minimization, the generated model was evaluated for geometric consistency, rotamer use, and atom clashes, showing to be of high quality. Almost all the sequence differences involve residues in the surface, and the hydrophobic core is almost identical in the two proteins. Therefore, our previous description of the tertiary structure of MPE ICA512 [19-20] likely applies to the description of MPE phogrin. Briefly, both proteins exhibit a typical ferredoxin-like (βαββαβ) fold [41], which is characterized by having a four-stranded antiparallel β sheet covered on one of its faces by two antiparallel α helices (Fig. 7).

Although we show in this work that MPE phogrin is a monomer in solution, to facilitate the comparison between the two proteins and help to follow the ensuing description of the results, MPE phogrin monomers in (Fig. 7) are shown in the orientation that they would adopt if they associated as suggested by the x-ray structure of MPE ICA512. In addition, and also to facilitate the comparisons, the residue numbering of MPE ICA512 was adopted here for MPE phogrin (see (Fig. **S1**) of Supplementary Data).

As mentioned in the introduction, both full length receptors inserted in the membrane have the potential to dimerize or form higher order aggregates. *In vitro*, the x-ray study of MPE ICA 512 at different pH identified two kind of dimers that might be relevant: one, named β4-β4 is formed by antiparallel pairing of strands β4 and helices α2; the other, named β2-β2, results from antiparallel pairing of strands β2 and helices α1. Since MPE phogrin is monomeric in solution, next we analyze in detail which structural features are likely to explain its behavior.

The following pieces of information are relevant for the analysis: (*i*) there are three β4-β4 dimer variants in MPE ICA512, populated at different pH and unit cells [19-20]; (*ii*) it was determined that unglycosylated MPE ICA512 *in vitro* only populates significantly the β2-β2 dimer [19]; (*iii*) glycosylation at Asn 506 in MPE ICA512 [42] is likely to hinder the formation of the β2-β2 dimer *in vivo*, and such glycosylation is not possible in MPE phogrin because Asn 506 is mutated to aspartic acid [8, 18]; (*iv*) both, MPE ICA512 and phogrin glycosylation at Asn 524 is sterically compatible with both dimers; and (*v*) the dimerization of the receptor is likely to involve the intracellular and transmembrane domains, which might provide most of the driving force for the association.

An inspection of the MPE phogrin monomers, arranged as if they were to associate in the manner of MPE ICA512,

Figure 7. Modeled 3D structure of MPE phogrin. Although MPE phogrin is monomeric in solution, here is depicted arranged in the two alternative dimeric forms found in the crystallographic unit cell of MPE ICA512 [19-20] to facilitate the comparison. The β4-β4 and β2-β2 dimers are shown in the top and bottom panels, respectively. Side chains of non-conserved residues (Fig. S1 in supporting information) are shown as sticks. Note that most changes are at the protein surface and also that the β4-β4 interface is evolutionarily much more preserved than the β2-β2 interface.

reveals a very strong sequence conservation of the residues at the putative β4-β4 interface (Fig. 7). Indeed, the interface is highly conserved in all the protein family (Fig. **S1**). There are only two sequence changes at the β4-β4 interface: A528E and Q532K. The changes are, however, compatible with the β4-β4 dimer observed in the crystallographic unit cell of ICA512 at pH 4.5 (Fig. 7). In addition, the change A528E introduces an additional interfacial hydrogen bond.

Side-chain differences between MPE ICA512 and MPE phogrin are much more abundant at the putative β2-β2 interface (Fig. 7). Four of the changes are particularly noteworthy. The first is N506D, which introduce a repulsive charge. The second is S508E, which also introduce negative charge repulsion and is at a position that showed to affect dimerization in ICA512 [19-20]. The last two are the mutations A484E and V487R, which would introduce steric constraints and charge repulsion. All together, these changes might explain the lack of dimerization *in vitro* of MPE phogrin.

ICA512 and phogrin are homologous proteins with a high degree of conservation throughout their entire se-

quences, and therefore it would be surprising if these receptors would display major differences in their quaternary structure, such as the assembly of the overall dimeric structure through different interfaces. The similarities and differences between the two proteins described so far allow speculating about the topology of the respective MPE domains when part of the membrane inserted receptor.

In vitro, unglycosylated MPE ICA512 dimerizes with a micromolar dissociation constant and through the β2-β2 interface, whereas the corresponding β4-β4 dimer is not significantly populated [19,20]. *In vivo*, however, glycosylated MPE ICA512 is unlikely to dimerize through the β2-β2 interface, for the bulky sugar moieties attached to residue 506 would clash. Indeed, no satisfactory solution could be found to the problem of accommodating the sugar moieties in a modeled β2-β2 dimer of MPE ICA512 (Ermácora *et al.* unpublished results). Thus, for this receptor variant, the β4-β4 dimer is the best candidate for relevance *in vivo*.

Nevertheless, the fact that the β4-β4 dimer is populated in neither of the variants in solution, suggests this association mode requires extra stabilization to materialize. The extra energy for populating the β4-β4 dimer seen in the MPE ICA512 x-ray structure may be provided by crystal packing forces; *in vivo*, the association may be driven by the interactions established by the other domains of the receptor and by the geometry of the interaction with the lipid bilayer.

In the case of MPE phogrin, β2-β2 dimerization is disallowed without the need of a post translational glycosylation. Therefore, it is conceivable that the two proteins may have evolved different strategies to override the tendency to the formation of a β2-β2 interface.

Finally, the geometry of the interaction with the membrane is a crucial factor for the determination of the *in vivo* topology of the receptor because the C-termini of the putative dimers must converge into a 2D surface to form the transmembrane segment. Unfortunately, all the attempts to obtain structural information on the connector segment (residues 560 to 576) failed because the full length mature extracellular region is self proteolyzed *in vitro* to finally yield the stable MPE domain [19]. Preliminary modeling studies indicate that the β4-β4 dimer allows a straightforward and structurally sound approach of its C-termini to the lipid bilayer, whereas a much more evolved arrangement of the connector region is needed in the case of the β2-β2 dimer (not shown).

3.6. Concluding Remarks

The physicochemical properties of MPE phogrin have been investigated. It is a stable protein domain, able to fold independently of the rest of the phogrin receptor. We show that the ectodomain is a monomer in solution and estimate the thermodynamic parameters of its folding. The study establishes several common features and specific differences between MPE phogrin and the homologous MPE ICA512, and given the biological importance and relatedness of the two proteins, the information obtained fills a gap in the current knowledge on their structure and dynamics. Also, the atomic details of the putative dimerization of MPE phogrin have been investigated by molecular modeling. This allowed the comparison with the experimentally determined structure of MPE ICA512. The gathered information is a starting point for modeling the entire receptor and design experiments to test its realization *in vivo*.

CONFLICT OF INTEREST

The authors confirm that this article content has no conflicts of interest.

ACKNOWLEDGEMENTS

This work was supported by grants from CONICET, UNQ, and ANPCyT

SUPPLEMENTARY MATERIAL

Fig. (**S1**): Alignment of MPE ICA512 and phogrin sequences

REFERENCES

[1] Caromile, L. A.; Oganesian, A.; Coats, S. A.; Seifert, R. A.; Bowen-Pope, D. F. The neurosecretory vesicle protein phogrin functions as a phosphatidylinositol phosphatase to regulate insulin secretion. *J. Biol. Chem.*, **2010**, *285*, 10487-10496.

[2] Lu, J.; Li, Q.; Xie, H.; Chen, Z. J.; Borovitskaya, A. E.; Maclaren, N. K.; Notkins, A. L.; Lan, M. S. Identification of a second transmembrane protein tyrosine phosphatase, IA-2beta, as an autoantigen in insulin-dependent diabetes mellitus: precursor of the 37-kDa tryptic fragment. *Proc. Natl. Acad. Sci. USA*, **1996**, *93*, 2307-2311.

[3] Solimena, M.; Dirkx, R., Jr.; Hermel, J. M.; Pleasic-Williams, S.; Shapiro, J. A.; Caron, L.; Rabin, D. U. ICA 512, an autoantigen of type I diabetes, is an intrinsic membrane protein of neurosecretory granules. *Embo J.*, **1996**, *15*, 2102-2114.

[4] Bottazzo, G. F.; Bosi, E.; Cull, C. A.; Bonifacio, E.; Locatelli, M.; Zimmet, P.; Mackay, I. R.; Holman, R. R. IA-2 antibody prevalence and risk assessment of early insulin requirement in subjects presenting with type 2 diabetes (UKPDS 71). *Diabetologia*, **2005**, *48*, 703-708.

[5] Trajkovski, M.; Mziaut, H.; Altkruger, A.; Ouwendijk, J.; Knoch, K. P.; Muller, S.; Solimena, M. Nuclear translocation of an ICA512 cytosolic fragment couples granule exocytosis and insulin expression in {beta}-cells. *J. Cell Biol.*, **2004**, *167*, 1063-1074.

[6] Suckale, J.; Solimena, M. The insulin secretory granule as a signaling hub. *Trends Endocrinol. Metab.*, **2010**, *21*, 599-609.

[7] Schubert, S.; Knoch, K. P.; Ouwendijk, J.; Mohammed, S.; Bodrov, Y.; Jager, M.; Altkruger, A.; Wegbrod, C.; Adams, M. E.; Kim, Y.; Froehner, S. C.; Jensen, O. N.; Kalaidzidis, Y.; Solimena, M. beta2-Syntrophin is a Cdk5 substrate that restrains the motility of insulin secretory granules. *PLoS One*, **2010**, *5*.

[8] Torii, S. Expression and function of IA-2 family proteins, unique neuroendocrine-specific protein-tyrosine phosphatases. *Endocr. J.*, **2009**, *56*, 639-648.

[9] Kubosaki, A.; Gross, S.; Miura, J.; Saeki, K.; Zhu, M.; Nakamura, S.; Hendriks, W.; Notkins, A. L. Targeted Disruption of the IA-2β Gene Causes Glucose Intolerance and Impairs Insulin Secretion but Does Not Prevent the Development of Diabetes in NOD Mice. *Diabetes*, **2004**, *53*, 1684-1691.

[10] Saeki, K.; Zhu, M.; Kubosaki, A.; Xie, J.; Lan, M. S.; Notkins, A. L. Targeted disruption of the protein tyrosine phosphatase-like molecule IA-2 results in alterations in glucose tolerance tests and insulin secretion. *Diabetes*, **2002**, *51*, 1842-1850.

[11] Kubosaki, A.; Nakamura, S.; Notkins, A. L. Dense core vesicle proteins IA-2 and IA-2beta: metabolic alterations in double knockout mice. *Diabetes*, **2005**, *54*, S46-51.

[12] Kubosaki, A.; Nakamura, S.; Clark, A.; Morris, J. F.; Notkins, A. L. Disruption of the transmembrane dense core vesicle proteins IA-2 and IA-2beta causes female infertility. *Endocrinology*, **2006**, *147*, 811-815.

[13] Roberts, C.; Roberts, G. A.; Lobner, K.; Bearzatto, M.; Clark, A.; Bonifacio, E.; Christie, M. R. Expression of the protein tyrosine phosphatase-like protein IA-2 during pancreatic islet development. *J. Histochem. Cytochem.*, **2001**, *49*, 767-776.

[14] Shimizu, S.; Saito, N.; Kubosaki, A.; SungWook, S.; Takeyama, N.; Sakamoto, T.; Matsumoto, Y.; Saeki, K.; Onodera, T. Developmental expression and localization of IA-2 mRNA in mouse neuroendocrine tissues. *Biochem. Biophys. Res. Commun.*, **2001**, *288*, 165-171.

[15] Lobner, K.; Steinbrenner, H.; Roberts, G. A.; Ling, Z.; Huang, G. C.; Piquer, S.; Pipeleers, D. G.; Seissler, J.; Christie, M. R. Different regulated expression of the tyrosine phosphatase-like proteins IA-2 and phogrin by glucose and insulin in pancreatic islets: relationship to development of insulin secretory responses in early life. *Diabetes*, **2002**, *51*, 2982-2988.

[16] Seissler, J.; Nguyen, T. B.; Aust, G.; Steinbrenner, H.; Scherbaum, W. A. Regulation of the diabetes-associated autoantigen IA-2 in INS-1 pancreatic beta-cells. *Diabetes*, **2000**, *49*, 1137-1141.

[17] Steinbrenner, H.; Nguyen, T. B.; Wohlrab, U.; Scherbaum, W. A.; Seissler, J. Effect of proinflammatory cytokines on gene expression of the diabetes-associated autoantigen IA-2 in INS-1 cells. *Endocrinology*, **2002**, *143*, 3839-3845.

[18] Kawakami, T.; Saeki, K.; Takeyama, N.; Wu, G.; Sakudo, A.; Matsumoto, Y.; Hayashi, T.; Onodera, T. Detection of proteolytic cleavages of diabetes-associated protein IA-2 beta in the pancreas and the brain using novel anti-IA-2 beta monoclonal antibodies. *Int. J. Mol. Med.*, **2007**, *20*, 177-185.

[19] Primo, M. E.; Klinke, S.; Sica, M. P.; Goldbaum, F. A.; Jakoncic, J.; Poskus, E.; Ermácora, M. R. Structure of the mature ectodomain of the human receptor-type protein-tyrosine phosphatase IA-2. *J. Biol. Chem.*, **2008**, *283*, 4674-4681.

[20] Primo, M. E.; Jakoncic, J.; Noguera, M. E.; Risso, V. A.; Sosa, L.; Sica, M. P.; Solimena, M.; Poskus, E.; Ermácora, M. R. Protein-protein interactions in crystals of the human receptor-type protein tyrosine phosphatase ICA512 ectodomain. *PLoS One*, **2011**, *6*, 15.

[21] Bork, P.; Patthy, L. The SEA module: a new extracellular domain associated with O-glycosylation. *Protein Sci.*, **1995**, *4*, 1421-1425.

[22] Andersen, J. N.; Jansen, P. G.; Echwald, S. M.; Mortensen, O. H.; Fukada, T.; Del Vecchio, R.; Tonks, N. K.; Moller, N. P. A genomic perspective on protein tyrosine phosphatases: gene structure, pseudogenes, and genetic disease linkage. *Faseb J.*, **2004**, *18*, 8-30.

[23] Brady-Kalnay, S. M.; Tonks, N. K. Protein tyrosine phosphatases as adhesion receptors. *Curr. Opin. Cell Biol.*, **1995**, *7*, 650-657.

[24] Chin, C. N.; Sachs, J. N.; Engelman, D. M. Transmembrane homodimerization of receptor-like protein tyrosine phosphatases. *FEBS Lett.*, **2005**, *579*, 3855-3858.

[25] Gross, S.; Blanchetot, C.; Schepens, J.; Albet, S.; Lammers, R.; den Hertog, J.; Hendriks, W. Multimerization of the protein-tyrosine phosphatase (PTP)-like insulin-dependent diabetes mellitus autoantigens IA-2 and IA-2beta with receptor PTPs (RPTPs). Inhibition of RPTPalpha enzymatic activity. *J. Biol. Chem.*, **2002**, *277*, 48139-48145.

[26] Primo, M. E.; Sica, M. P.; Risso, V. A.; Poskus, E.; Ermácora, M. R. Expression and physicochemical characterization of an extracellular segment of the receptor protein tyrosine phosphatase IA-2. *Biochim. Biophys. Acta*, **2006**, *2*, 174-181.

[27] Schagger, H.; von Jagow, G. Tricine-sodium dodecyl sulfate-polyacrylamide gel electrophoresis for the separation of proteins in the range from 1 to 100 kDa. *Anal. Biochem.*, **1987**, *166*, 368-379.

[28] Gill, S. C.; von Hippel, P. H. Calculation of protein extinction coefficients from amino acid sequence data. *Anal. Biochem.*, **1989**, *182*, 319-326.

[29] Clerico, E. M.; Ermácora, M. R. Tryptophan mutants of intestinal fatty acid-binding protein: ultraviolet absorption and circular dichroism studies. *Arch. Biochem. Biophys.*, **2001**, *395*, 215-224.

[30] Uversky, V. N. Use of fast protein size-exclusion liquid chromatography to study the unfolding of proteins which denature through the molten globule. *Biochemistry*, **1993**, *32*, 13288-13298.

[31] Motulsky, H.; Christopoulos, A. *Fitting Models to Biological Data Using Linear and Nonlinear Regression: A Practical Guide to Curve Fitting*, second ed.; GraphPad Sotware Inc.: San Diego, 2003.

[32] Kawasaki, E.; Hutton, J. C.; Eisenbarth, G. S. Molecular cloning and characterization of the human transmembrane protein tyrosine phosphatase homologue, phogrin, an autoantigen of type 1 diabetes. *Biochem. Biophys. Res. Commun.*, **1996**, *227*, 440-447.

[33] Savitzky, A.; Golay, M. J. E. Smoothing and Differentiation of Data by Simplified Least Squares Procedures. *Anal. Chem.*, **1964**, *36*, 1627-1639.

[34] Deleage, G.; Geourjon, C. An interactive graphic program for calculating the secondary structure content of proteins from circular dichroism spectrum. *Comput. Appl. Biosci.*, **1993**, *9*, 197-199.

[35] Pace, C. N. Determination and analysis of urea and guanidine hydrochloride denaturation curves. *Methods in enzymology*, **1986**, *131*, 266-280.

[36] Privalov, P. L. Stability of proteins: small globular proteins. *Adv. Protein Chem.*, **1979**, *33*, 167-241.

[37] Emsley, P.; Cowtan, K. Coot: model-building tools for molecular graphics. *Acta. Crystallogr. D Biol. Crystallogr.*, **2004**, *60*, 2126-2132.

[38] Laskowski, R. A.; MacArthur, M. W.; Moss, D. S.; Thornton, J. M. PROCHECK: a program to check the stereochemical quality of protein structures. *J. Appl. Cryst.*, **1993**, *26*, 283-291.

[39] Chen, V. B.; Arendall, W. B., 3rd; Headd, J. J.; Keedy, D. A.; Immormino, R. M.; Kapral, G. J.; Murray, L. W.; Richardson, J. S.; Richardson, D. C. MolProbity: all-atom structure validation for macromolecular crystallography. *Acta Crystallogr. D Biol. Crystallogr.*, **2010**, *66*, 12-21.

[40] Myers, J. K.; Pace, C. N.; Scholtz, J. M. Denaturant m values and heat capacity changes: relation to changes in accessible surface areas of protein unfolding. *Protein Sci.*, **1995**, *4*, 2138-2148.

[41] Hubbard, T. J.; Murzin, A. G.; Brenner, S. E.; Chothia, C. SCOP: a structural classification of proteins database. *Nucleic Acids Res.*, **1997**, *25*, 236-239.

[42] Hermel, J. M.; Dirkx, R., Jr.; Solimena, M. Post-translational modifications of ICA512, a receptor tyrosine phosphatase-like protein of secretory granules. *Eur. J. Neurosci.*, **1999**, *11*, 2609-2620.

Received: July 21, 2012 **Revised: August 25, 2012** **Accepted: September 10, 2012**